Climatology of Low-Level Clouds over Western Equatorial Africa Based on Ground Observations and Satellites

O. CHAMPAGNE,[a] R. AELLIG,[b] A. H. FINK,[b] N. PHILIPPON,[a] P. CAMBERLIN,[c] V. MORON,[d] P. KNIPPERTZ,[b] G. SEZE,[e] AND R. VAN DER LINDEN[b]

[a] *Institut des Géosciences de l'Environnement, Université Grenoble Alpes, CNRS, Grenoble, France*
[b] *Institute of Meteorology and Climate Research, Karlsruhe Institute of Technology, Karlsruhe, Germany*
[c] *Centre de Recherches de Climatologie, UMR 6282 Biogéosciences, CNRS/Université de Bourgogne Franche-Comté, Dijon, France*
[d] *Aix Marseille Université, CNRS, IRD, INRA, Coll France, CEREGE, Aix-en-Provence, France*
[e] *LMD, IPSL, UPMC, CNRS, EP, ENS, Paris, France*

(Manuscript received 13 May 2022, in final form 17 February 2023, accepted 22 February 2023)

ABSTRACT: The tropical cloud forest ecosystem in western equatorial Africa (WEA) is known to be sensitive to the presence of an extensive and persistent low-level stratiform cloud deck during the long dry season from June to September (JJAS). Here, we present a new climatology of the diurnal cycle of the low-level cloud cover from surface synoptic stations over WEA during JJAS 1971–2019. For the period JJAS 2008–19, we also utilized estimates of cloudiness from four satellite products, namely, the Satellite Application Facility on Support to Nowcasting and Very Short Range Forecasting (SAFNWC) cloud classification, the Day and Night Microphysical Schemes (DMS/NMS), and cross sections from *CALIPSO* and *CloudSat* (2B-GEOPROF-lidar). A comparison with surface stations reveals that the NMS at night together with SAFNWC at daytime yield the smallest biases. The climatological analysis reveals that low-level clouds persist during the day over the coastal plains and windward side of the low mountain ranges. Conversely, on their leeward sides, i.e., over the plateaus, a decrease of the low-level cloud frequency is observed in the afternoon, together with a change from stratocumulus to cumulus. At night, the low-level cloud deck reforms over this region with the largest cloud occurrence frequencies in the morning. Vertical profiles from 2B-GEOPROF-lidar reveal cloud tops below 3000 m even at daytime. The station data and the suitable satellite products form the basis to better understand the physical processes controlling the clouds and to evaluate cloudiness from reanalyses and models.

KEYWORDS: Atmosphere; Africa; Cloud cover; Climatology; Satellite observations; Surface observations

1. Introduction

Many tropical wet forest ecosystems are tightly linked to the presence of low-level clouds. These clouds reduce water demand and favor photosynthesis by enhancing diffuse radiation (Karger et al. 2021), and in montane cloud forests they result in occult rainfall through leaf wetting (Berry and Goldsmith 2020; Goldsmith et al. 2013). Western equatorial Africa (WEA) encompasses southern Cameroon, Gabon, and the Republic of Congo and comprises the Ogooué and Kioulou–Niari basins as well as the Cristal and Chaillu Mountains and Batéké Plateau (Fig. 1). It harbors large expanses of dense, evergreen to semievergreen rain forests, whose presence is associated with a very high intra-annual and interannual stability of the cloud cover (Wilson and Jetz 2016). Philippon et al. (2019, 2022) have provided evidence of low solar irradiance, sunshine duration, and potential evapotranspiration levels during the main dry season (June–September, JJAS) due to persistent low-level clouds. Recent studies suggest a potential climate change threat on this forested region (Oliveira et al. 2014), and mainly a drying trend in Gabon (Bush et al. 2020) and an increase in shortwave radiation farther east in the Congo basin (Burnett et al. 2020). Moreover, the years with very warm sea surface temperatures in the eastern Atlantic favored less stratiform clouds in Gabon (Maley and Hilaire 1993). Further back, a strengthening of El Niño–Southern Oscillation (ENSO) variability likely forced the WEA rain forest to retreat 2000 years ago (Bayon et al. 2019). This past retreat suggests a general vulnerability of this forest to climatic variations. A potential threat through the ongoing climate change motivates the research on low-level clouds in this region.

Despite these recent climatic trends and the potential high vulnerability of WEA forests under climate change, very few studies have focused on the low-level clouds in WEA in contrast to some neighboring regions such as the southeastern tropical and subtropical Atlantic Ocean (Wood et al. 2012; Wood 2012; Painemal et al. 2015), southern West Africa (SWA; Kalthoff et al. 2018; Knippertz et al. 2011; Lohou et al. 2020; Schrage and Fink 2012; Schuster et al. 2013; van der Linden et al. 2015) or the Namib Desert in western South Africa (Andersen and Cermak 2018; Andersen et al. 2019, 2020). The southeastern tropical and subtropical Atlantic Ocean is covered by an extensive layer of marine stratus at the low-level inversion (Wood

O. Champagne and R. Aellig contributed equally to the manuscript.

Supplemental information related to this paper is available at the Journals Online website: https://doi.org/10.1175/JCLI-D-22-0364.s1.

Corresponding author: Olivier Champagne, olivier.champagne@univ-grenoble-alpes.fr

DOI: 10.1175/JCLI-D-22-0364.1

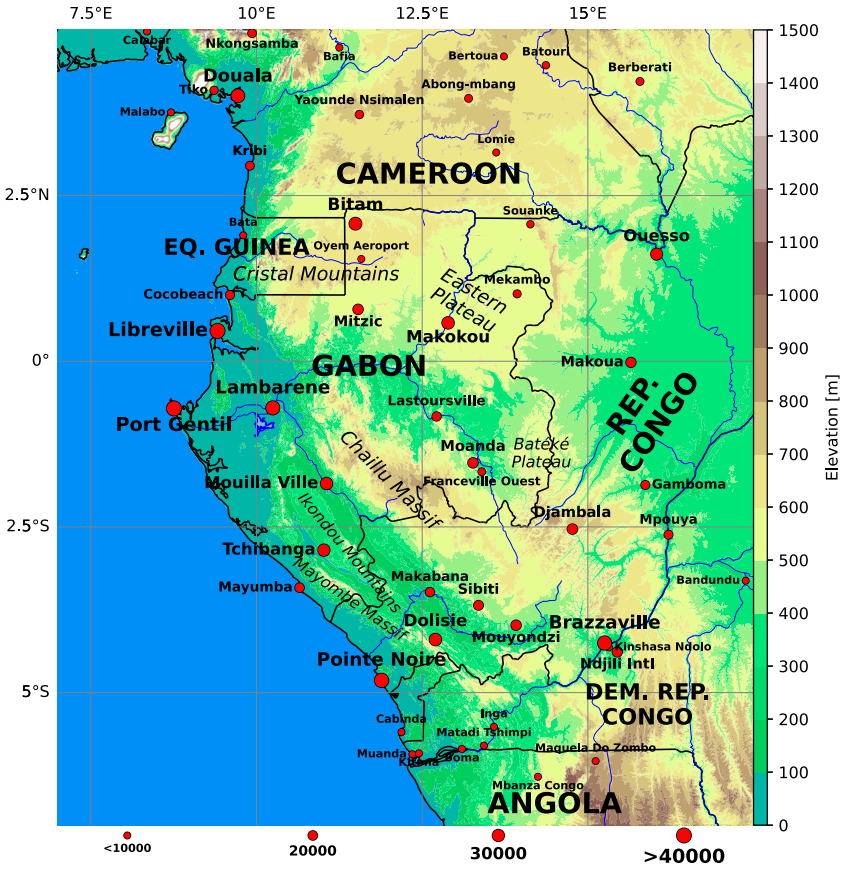

FIG. 1. Study region, names of main mountain ranges (terrain elevation; in m; from Danielson and Gesch 2011) and location of stations used. The station marker size is proportional to the total number of 3-hourly low-level cloud-cover observations available in the period 1971–2019.

2012; Painemal et al. 2015). This is particularly so in boreal summer, when the coastal upwelling extends northward to Cape Lopez (0°37′S) and the equatorial upwelling cools the eastern equatorial Atlantic Ocean (Adebiyi and Zuidema 2018; Fuchs et al. 2018; Hu et al. 2008). In SWA, low-level clouds are mainly present during the JJAS monsoon season. At night the low-level clouds rapidly expand from the coast inland and peak in the morning hours covering an area of nearly 800 000 km^2 (van der Linden et al. 2015). The processes involved in the nighttime genesis and daytime lysis of the low-level clouds involves a complicated multiphase balance between cold air advection from the Atlantic Ocean and divergence of net radiation and turbulent fluxes, partly in association with a developing nighttime low-level jet (Knippertz et al. 2015; Lohou et al. 2020). On the contrary, in the Namib region, low-level clouds form over the ocean during the night, are advected to the land, and dissipate quickly in the morning (Andersen et al. 2020).

While the relative roles of cloud advection from the nearby Atlantic Ocean, orographic cloud genesis, and boundary layer processes have not been assessed thoroughly for WEA yet, the very first climatology of low-level clouds was presented in Dommo et al. (2018). They used station observations, satellite data, and the European Centre for Medium-Range Weather Forecasts interim reanalysis (Dee et al. 2011) to show that dry season low-level cloud cover is developing in May, peaks in July–August, and then decreases again in October. These clouds tend to be more present in the morning, similarly to what has been described for SWA (van der Linden et al. 2015). The low-level clouds are more prevalent in the coastal plains and decrease inland, likely associated with a foehn effect leeward of the Chaillu Mountains, Cristal Mountains, and Batéké Plateau (Fig. 1) leading to dissipation of the cloud deck associated with the southwesterly to westerly low-level winds. The formation of low-level clouds could also be favored by biomass burning aerosols that increase airmass stability (Solmon et al. 2021; Mallet et al. 2021).

Dommo et al. (2018) use the cloud classification from the Satellite Application Facility on Support to Nowcasting and Very Short Range Forecasting (SAFNWC; Derrien and Le Gléau 2005), which has the advantage of a high spatial and temporal resolution and was previously used to describe daytime low-level clouds in SWA (van der Linden et al. 2015). However, SAFNWC has difficulties detecting very low-level clouds at night (van der Linden et al. 2015) and a validation against in situ synoptic observations was not performed

extensively in Dommo et al. (2018). Thus, the goal of the present study is to complement and expand on the study by Dommo et al. (2018). In particular, our study relies on an improved database for in situ observations of clouds which contains more stations (62) over a longer period (1971–2019). The spatial sampling is therefore increased, giving a better view of the low-level cloud-cover spatial pattern and conferring robustness to our results. The longer overlap period between in situ observations and satellite estimates (2008–19 against 2008/09 in Dommo et al. 2018) enables computing scores of performance, thus quantitatively evaluating the satellites datasets. In addition, we consider eight genera of low-level clouds and not only the total low-level cloud cover as in Dommo et al. (2018). This allows us to precisely document (i) the evolution from one genus to another along the diurnal cycle and (ii) how well these different genera are detected by satellites. Last, we worked with (i) day and night microphysical schemes (NMS/DMS; Lensky and Rosenfeld 2008) to obtain a more accurate representation of the diurnal cycle of the low-level cloud cover and (ii) *CALIPSO*/Cloud-Aerosol Lidar with Orthogonal Polarization (CALIOP) data (viz., the 2B-GEOPROF-lidar product; Mace and Zhang 2014) to infer the cloud cover vertical profile and cases when low-level clouds are under a multilayered cover.

These points serve the overall goal of our study to present a description of the diurnal cycle of the long dry season low-level cloud cover over WEA. It should also provide a baseline to further investigate low-level clouds variability in the region as well as their realism in global and regional climate model simulations.

Section 2 will introduce the new set of in situ observations and the satellite datasets, section 3 will present an extensive comparison between low-level clouds from SYNOP observations and from satellite data, and section 4 will discuss and summarize the main findings.

2. Data and methods

a. *A comprehensive new dataset of cloud observations from stations*

The primary source of observed low-level cloud cover, including the low-level cloud fraction (LCF) and the low-level cloud genus (LCG), is the Extended Edited Synoptic Cloud Reports Archive (EECRA; Hahn et al. 1999; Eastman and Warren 2014) covering the period until 2009. LCF is expressed in oktas and is of particular interest from a regional climate perspective as it governs radiation reaching the surface. LCG uses the World Meteorological Organization (WMO) coding into nine types (WMO 2019) plus two EECRA-specific types (11 = obscure sky with fog; 10 = thunderstorm with showers). These two latter types were omitted in this study (LCF coded to 0) because they result from ancillary information specific to EECRA and are not available in other datasets described below. The WMO low-level cloud coding comprises cumulus (01 and 02), stratocumulus (04 and 05), stratus (06 and 07), cumulus and stratocumulus (08), and cumulonimbus (03 and 09). In total, 62 stations were extracted from EECRA for the period 1971–2009 and the region 5°N–6.5°S, 6.5°–16.5°E (Fig. 1). To fill in gaps and to update the EECRA database to 2019, three other databases were used; these are in order of priority: the Met Office Integrated Data Archive System (MIDAS; Met Office 2012), the Integrated surface database (ISD; Smith et al. 2011), and the African Monsoon Multidisciplinary Analyses Information System (AMMA; Fleury et al. 2011). MIDAS is less extensively used than EECRA but a data quality check (not shown) has revealed better consistency of MIDAS compared to ISD and AMMA, in respect to EECRA. ISD had some decoding problems from 2013, while our quality control led us to conclude that AMMA should be given the lowest priority. EECRA and the three additional sources are based on the same in situ stations and are therefore consistent in their common periods of records, as shown with the example of Libreville (Fig. S1 in the online supplemental material). From the latter three additional sources, three stations not in EECRA were added: Franceville-Mvengue and Oyem (both in Gabon) and Mbanza Kongo (in Angola). Inconsistent reports, where either LCG or LCF was zero and the respective other variable was nonzero, were omitted. We also checked if the cloud observations could be enhanced by hourly meteorological aerodrome reports (METAR) at airports, but unfortunately the cloud type coding is different and cloud fraction is not provided in oktas (Fig. S1). Nevertheless, our merged in situ cloud observations at synoptic stations (SYNOP observations) are longer and more complete than the in situ observations used in Dommo et al. (2018). The observations have been homogenized with a Standard Normal Homogeneity Test (Alexandersson and Moberg 1997) and a visual inspection of the data. The SYNOP observations have been published in open access alongside this article (Aellig et al. 2022).

SYNOP observations are carried out by trained observers eight times a day at main (0000, 0600, 1200, and 1800 UTC) and intermediate (0300, 0900, 1500, and 2100 UTC) synoptic hours. Note that the local time is UTC + 1 h. The location of stations, the total number of observations available, and their temporal evolution for each source and observation time can be inferred from Fig. 2. Overall, the number of available observations decreased over time but increased again in the late 2000s. Stations in Gabon and Republic of Congo (RC) are the best documented, matching with the cloudiest region of WEA (Dommo et al. 2018; Philippon et al. 2019). Generally, more daytime (Figs. 2c,d,i,j) than nighttime (Figs. 2a,b,k,l) recordings were available due to daytime-only operations at several stations.

b. *Satellite products*

1) CLOUD TYPE FROM SAFNWC

The cloud type (CT) product from SAFNWC consists of a classification into 14 types available at 3-km spatial and 15-min temporal resolutions over Europe and Africa from 2008 to 2019 (Derrien and Le Gléau 2005). This product is based on the Spinning Enhanced Visible and Infrared Imager (SEVIRI), a passive sensor with 12 different spectral channels on board the Meteosat Second Generation geostationary

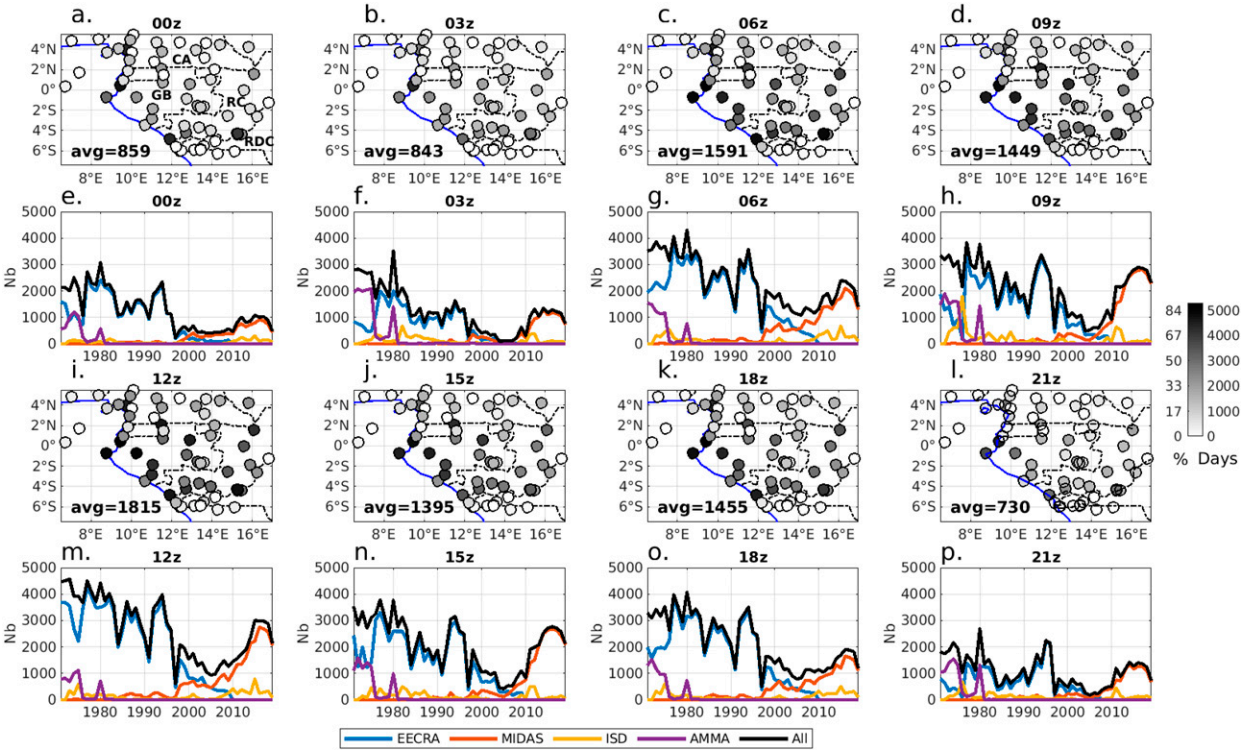

FIG. 2. (a)–(d),(i)–(l) Number of JJAS observations available per stations at 3-hourly time steps (maps). The average number of observations for all stations is depicted in the bottom-left corner. (e)–(h),(m)–(p) Total number of JJAS observations (all stations) per year and data source at 3-hourly time steps for 1971–2019 (line graphs). Letters in (a) indicate country names: CA = Cameroon; GB = Gabon; RC = Republic of the Congo; RDC = Democratic Republic of the Congo.

satellite (Schmetz et al. 2002). To construct the SAFNWC CT product, cloud detection and cloud type classification are performed using series of threshold tests applied sequentially: tests on reflectance and window channel brightness temperature at 10.8 μm and differences in brightness temperature between two wavelengths (chosen among 10.8, 12, 3.9, and 8.7 μm). The used thresholds depend on illumination, viewing geometry and geographical location, and are computed from a radiative transfer model using ancillary data. Additional tests on spatial and temporal variability of the brightness temperature at 10.8 μm and spatial variability of the reflectance are also used. A detailed description of the SAFNWC CT algorithm can be found in Derrien et al. (2013).

In our study, SAFNWC CTs are extracted for the WEA domain covering 5°N–6.5°S, 6.5°–16.5°E and the 2008–19 period. For simplification and following Dommo et al. (2018), the 14 CTs were recombined into seven CTs: cloud-free, very low clouds [up to 2000 m above mean sea level (MSL)], low clouds (2000–3500 m MSL), midlevel clouds (3500–6500 m MSL), high opaque clouds, high semitransparent clouds (the latter two higher than 6500 m MSL), and finally fractional clouds (i.e., small cumulus, thin low or midlevel cloud fractions, very thin high cloud fractions, broken and thin midlevel and low-level clouds). Cloud type maps with the seven types are shown as examples in Figs. 3b and 3e for 1200 UTC 21 August 2015 and 0000 UTC 11 July 2010.

2) NIGHT AND DAY MICROPHYSICAL SCHEMES

The Night Microphysical Scheme (NMS) and the Day Microphysical Scheme (DMS) are based on radiances and reflectances in the visible and infrared (IR) channels of SEVIRI (Lensky and Rosenfeld 2008; Schmetz et al. 2002). The schemes are based on three different channel combinations, which are combined to red–green–blue (RGB) composites. The DMS is a combination of the solar reflectance in the visible channel at 0.8 μm (red) and at 3.9 μm (green), and of the brightness temperature of the IR channel at 10.8 μm (blue). The 0.8 μm channel is a measure of the cloud optical depth and amount of cloud water and ice. The 3.9 μm visible channel is a qualitative measure for cloud particle size and phase (Lensky and Rosenfeld 2008). The NMS uses the difference of the brightness temperatures of the IR channels between 10.8 and 12.0 μm (red), and between 3.9 and 10.8 μm (green), and the brightness temperature of the IR channel at 10.8 μm represented in blue (Lensky and Rosenfeld 2008). The channels represented with green are sensitive to particle size of hydrometeors and the channels represented in red are a measure of the opaqueness of clouds. Figures 3a and 3d show examples of DMS and NMS for 1200 UTC 21 August 2015 and 0000 UTC 11 July 2010 with the RGB NMS and DMS cloud classification by EUMeTrain (2017). From these schemes, we distinguish for every grid point (3 km × 3 km) three categories:

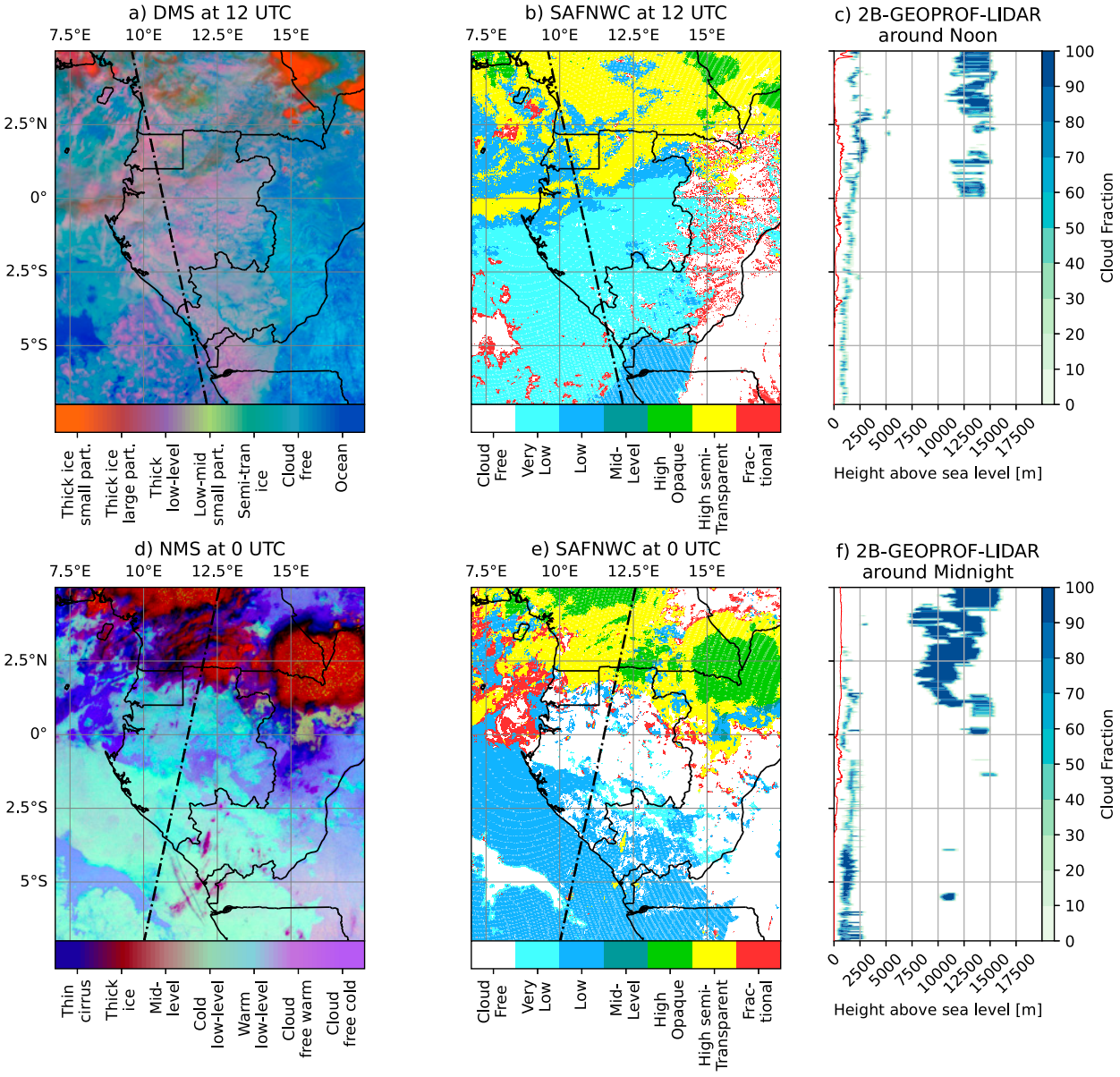

FIG. 3. Satellite products on (a)–(c) 1200 UTC 21 Aug 2015 and (d)–(f) 0000 UTC 11 Jul 2010 representing cloud types from (a) Day Microphysical Scheme, (d) Night Microphysical Scheme, (b),(e) SAFNWC and (c),(f) cloud height and fraction from 2B-GEOPROF-lidar. The black dotted line in (a), (b), (d), and (e) depicts the path of the satellite, the data of which are shown in (c) and (f). The red line in (c) and (f) represents the elevation.

low clouds, higher clouds, and clear skies. The low-level cloud cover in DMS is determined by a reflectance of more than 25% in the 0.8 μm visible channel and a brightness temperature (10.8 μm) greater than 283 K, while during the night the low-level cloud cover in the NMS is determined by a difference between the brightness temperature of the channels 3.9 and 10.8 μm greater than 2 K and a brightness temperature of channel 10.8 μm greater than 283 K. The thresholds for NMS to detect low-level cloud cover have been used already in former studies (van der Linden et al. 2015). 283 K represents the temperature at about 3000 m MSL in the study region, likely the upper limit of low-level clouds. In both DMS and NMS, brightness temperatures lower than 283 K are considered as higher clouds.

3) *CloudSat*/*CALIPSO* CPR/CALIOP (2B-GEOPROF-LIDAR)

The 2B-GEOPROF-lidar product is a merged product of data from the CALIOP lidar aboard *CALIPSO* (Winker et al. 2003) and the Cloud Profiling Radar (CPR) aboard *CloudSat* (Stephens et al. 2002). Mace and Zhang (2014) developed the 2B-GEOPROF-lidar product combining both profiles, getting

the most out of the information from both satellites. These two satellites are in the A-Train constellation circling around Earth in about 90 min and having a repeat period of 16 days until they sample the same swath again. They scan WEA on an ascending path from the southeast to the northwest between 1220 and 1315 UTC, and on a descending path from the northeast to the southwest between 2320 and 0015 UTC. The time periods available were JJAS 2006–17 for daytime and JJAS 2006–10 for nighttime. The CPR can penetrate more optically thick clouds, while CALIOP can detect thin clouds and clouds close to the surface (Mace et al. 2009; Marchand et al. 2008). An illustrative example for West Africa is given in Knippertz et al. (2011). 2B-GEOPROF-lidar has a spatial resolution of around 1.4 km along track, about 1.8 km cross track, and about 250 m vertically (Mace et al. 2009). In WEA, the swaths have a zonal distance of around 170 km between each other.

4) Spatial representation of the three satellite products

To qualitatively illustrate the performance of the different satellite products at day and night, Fig. 3 provides examples for 1200 UTC 21 August 2015 and 0000 UTC 11 July 2010. At daytime (top panels), both the SAFNWC and DMS represent the low-level clouds over Gabon and the adjacent ocean similarly. In the 2B-GEOPROF-lidar product, the high clouds over Cameroon and northern Gabon, likely stemming from deep convection, are represented by high opaque and semitransparent clouds in SAFNWC. At night (bottom panels), the difficulty in the detection of low-level clouds by SAFNWC as opposed to NMS is clearly visible over central and northern Gabon. 2B-GEOPROF-lidar shows the thickened high-level clouds over the northern part of the region, which potentially prevents detection of low-level clouds underneath. A close inspection of Fig. 3f reveals that 2B-GEOPROF-lidar can detect low-level clouds underneath higher clouds, if the latter are thin.

5) Climatology of low-level cloud cover from satellites

The climatology of low-level cloud cover was calculated for SAFNWC, DMS, NMS, and 2B-GEOPROF-lidar. These raw products do not provide LCF data (except for 2B-GEOPROF-lidar), since only the presence or absence of clouds in each pixel is detected. Hence, the climatology was primarily based on the low-level cloud occurrence frequency (LCOF).

For SAFNWC, we calculated the average JJAS 3-hourly LCOF for the very low and low-level cloud types at each grid point. Very low clouds (top of the cloud under 2000 m MSL) and low clouds (2000–3500 m MSL) types are considered together for the calculation of LCOF because the top of the low-level clouds detected in SYNOP (i.e., stratocumulus) can be situated above 2000 m MSL. This choice highlights the difficulty of comparing low-level clouds from ground observations and from satellites. At stations, clouds are seen from the ground and therefore determined according to their base height (low, middle, or high level) and type (nine possible categories). Cumulonimbus clouds are for instance reported by WMO as low clouds (i.e., with a base height below 2000 m MSL) despite their vertical extension. With satellites, clouds are determined according to their top height, so cumuliform clouds are often classified as higher clouds and low clouds are masked in case of a multilayered cloud cover. Therefore, the mismatch between ground observations and satellite estimates of low-level clouds can be quite large in the presence of cumulus, cumulonimbus, or a multilayered cloud cover. The grid points characterized by fractional clouds were also reassigned to one of the other cloud type when at least half of the eight surrounding points belonged to that other type, following the method in Dommo et al. (2018). This reassignment was made because the number of fractional clouds is not negligible, and this type appears spatially as a transition between two types (cf. Fig. 3). LCOF at each grid point and observation time was obtained by calculating the ratio of the number of occurrences of very low level, low level, or reassigned fractional days to the total number of days, excluding higher clouds (mid, high opaque, and high semitransparent). This method counters the problem of low-level clouds not detected due to clouds situated above. The higher-level cloud occurrence frequency was also calculated from the ratio of occurrence number of mid, high opaque, and high semitransparent cloud types to the total number of days.

For the climatology of low-level cloud cover based on NMS and DMS, we calculated for each grid point the average JJAS 3-hourly LCOF with the thresholds defined in section 2b(2), but only using the data with a threshold of the brightness temperature (10.8 μm) greater than 283 K. With this approach we alleviated the problem of clouds situated above the low-level clouds, similarly to the approach used to calculate LCOF from SAFNWC.

For the climatology of low-level cloud cover based on 2B-GEOPROF-lidar, we calculated first the cloud fraction and the cloud occurrence frequency at each vertical level (250 m resolution) and for each 0.5° parts (roughly 56 km) along track of the swaths [see section 2b(3)] using the random-overlap method (Geleyn and Hollingsworth 1979; Räisänen et al. 2004). For the lowest 3000 m MSL, we calculated the climatology of LCF and LCOF with the maximum-random-overlap method (Räisänen et al. 2004). These overlap assumptions follow the method used in van der Linden et al. (2015).

c. *Methods for comparing in situ observations and satellite products*

LCF and LCG at synoptic weather stations (SYNOP observations) are assessed by trained observers. Despite the subjective assessment and problems at night due to low illumination, various previous studies have shown their great value in obtaining cloud climatology and verification against satellite observations over Africa (van der Linden et al. 2015).

For the comparison with satellite products, the LCF climatology was calculated at synoptic weather station for time steps when LCG was either “stratocumulus” (genera 4 and 5), “stratus” (6 and 7), or “stratocumulus and cumulus” (8). For all other low-level cloud genera (1, 2, 3, 9, i.e., cumulus and

cumulonimbus clouds), the corresponding low-level cloud fraction was set to 0 oktas because these clouds are not strictly low-level clouds and are likely seen as higher clouds from the satellites. Note that genus 1 (cumulus humilis), is rare, as its frequency of occurrence is less than 2% at night and about 6% at daytime. Thus, using cloud genera 4–8 for stratiform low-level clouds at stations and comparing it with satellite low-level clouds appears to be a tolerable inconsistency. LCOF for SYNOP observations was calculated by counting the occurrence of LCF higher than 4 oktas. For the evaluation of satellite products against SYNOP observations, we converted cloud occurrence around SYNOP stations to cloud fraction. We took the distance-weighted (cosine function from 0 to $\pi/2$) average cloud fraction in a radius of 20 km around the station at the time of the observation, under the assumption that the observer on the ground can classify clouds and their fractional cover in the sky up to this distance (WMO 2019). For SAFNWC, very low clouds, low clouds and fractional reassigned clouds [see section 2b(5)] are considered together for the calculation of low cloud fraction, similarly to the calculation of LCOF described in section 2b(5). For the comparison of low-level cloud fraction from SYNOP observations and satellite data, days with more than 50% of higher clouds in the 20 km radius around a station were excluded from the analysis. This condition was applied because high- and midlevel clouds prevent the detection of lower clouds from the satellites.

3. Results

This section describes in four parts the diurnal cycle of low-level clouds in WEA. The first two parts explore the low-level cloud fraction and low-level cloud genus from SYNOP observations on the one hand and then the low-level cloud occurrence frequency from the three satellite datasets on the other hand. The third part shows a comparison between SYNOP observations and satellite data. The last part thoroughly compares the day and night evolution of low-level clouds from SYNOP observations and satellite data.

a. *Ground observations of low-level cloud fraction and genus*

The long-term (JJAS 1971–2019) mean diurnal cycle of LCF is provided in Fig. 4. LCF with stratiform clouds only (types 4–8, Figs. 4i–p) and with only cumuliform clouds (types 1–3 and 9, Figs. 4q–x) are also shown. Taking LCF calculated from all genera, the cloud fraction is clearly lower toward the Congo Basin in the east (Figs. 4a–h). In eastern Gabon, eastern Cameroon and southwestern RC, LCF increases at night (Figs. 4h,a,b), remains high until noon (Fig. 4e), and decreases in the afternoon (Figs. 4f–g). When taking stratiform clouds only, the decrease is more pronounced and occurs earlier in eastern Gabon and Cameroon (Figs. 4l–n), showing that these regions are affected by convection and the development of cumuliform clouds in the daytime (Figs. 4t–v).

The occurrence of cloud genus from SYNOP observations furnishes additional information regarding the type of low-level cloud cover in WEA (Fig. 5). Stratocumulus (Sc, genera 4 and 5) is by far the most frequent type at nighttime (1800–0300 UTC), representing two-thirds of all cloud genera (Figs. 5f–j). The second most frequent cloud genus at night is cumulonimbus (Cb, genera 3 and 9) occurring at 21.1% of all observations. During daylight (0600–1500 UTC, Figs. 5a–e), stratocumulus is less prominent than at night but remains the most frequent (44%) followed by "cumulus humilis" and "mediocris" (Cu, genera 1 and 2, 24.5%). The other main type is "cumulus and stratocumulus" (Cu and Sc, genus 8, 15.7%). Finally, the occurrence of stratus (St, genera 6 and 7) is very low (1%–3%) during day and night (Figs. 5d,i). These results show that a significant number of low-level clouds are convective (Cu and Cb represent together 37.5% of all genera during the day and 23.5% at night). However, the portion of the sky covered by Cu and Cb is generally lower than Sc (oktas, x axis of Fig. 5). Stratocumulus and stratus show a frequency distribution skewed to higher sky coverage (7–8 oktas, Figs. 5c,d,h,i). For cumulus, the distribution shows a higher frequency between 3 and 6 oktas and a distribution even skewed to lower cloud coverage (Fig. 5a). The distribution of cumulonimbus is centered around 4–7 oktas but is skewed to higher cloud coverage during the day (Fig. 5b) while the distribution is flatter at night (Fig. 5g).

The frequency of the cloud types varies spatially throughout the day (Fig. 6). At night (1800–0300 UTC), the frequency of stratocumulus (genera 4 and 5) is high (>70%) especially in western Cameroon, Gabon, and southwest RC. Some exceptions such as Port-Gentil (Fig. 1), show a lower amount of stratocumulus at night. The simultaneous higher amount of stratocumulus and cumulus (genus 8) at that station is probably due to the relatively warm ocean water and land friction, enhancing locally the transition from Sc to Cu. In the morning, the amount of Sc markedly decreases everywhere but stays relatively high in the central part of Gabon. Simultaneously, the amount of cumulus (genera 1 and 2) increases, especially in Cameroon and RC, where it reaches a maximum around 1200 UTC. The cumulus and stratocumulus genus (genus 8) also reaches a maximum around 1200 UTC, but occurs more frequently near the coast of Gabon. It reflects the breaking of the stratocumulus deck in the course of the day. Further, the stratus deck is more persistent on the windward slope of the Chaillu massif. The frequency of cumulonimbus (genera 3 and 9) increases later, reaching a maximum around 1800 UTC, located mostly in Cameroon and RC, while staying very low near the coast of Gabon and RC.

b. *Satellite observations of horizontal and vertical distributions of low-level clouds*

The average diurnal evolution of LCOF from SAFNWC, NMS, and DMS are displayed in Fig. 7 at the same 3-hourly time steps as in Fig. 4. Between 0600 and 0900 UTC, LCOF increases dramatically in both products (Figs. 7i,j,m,n), likely associated with the low solar angle that prevents the satellite from satisfactorily detecting low-level clouds just after sunrise. This effect is conspicuous in the first hour of daylight with a large LCOF increase observed between 0600 and 0700 UTC (Fig. S2). In DMS, the increase of LCOF continues between 0900 and

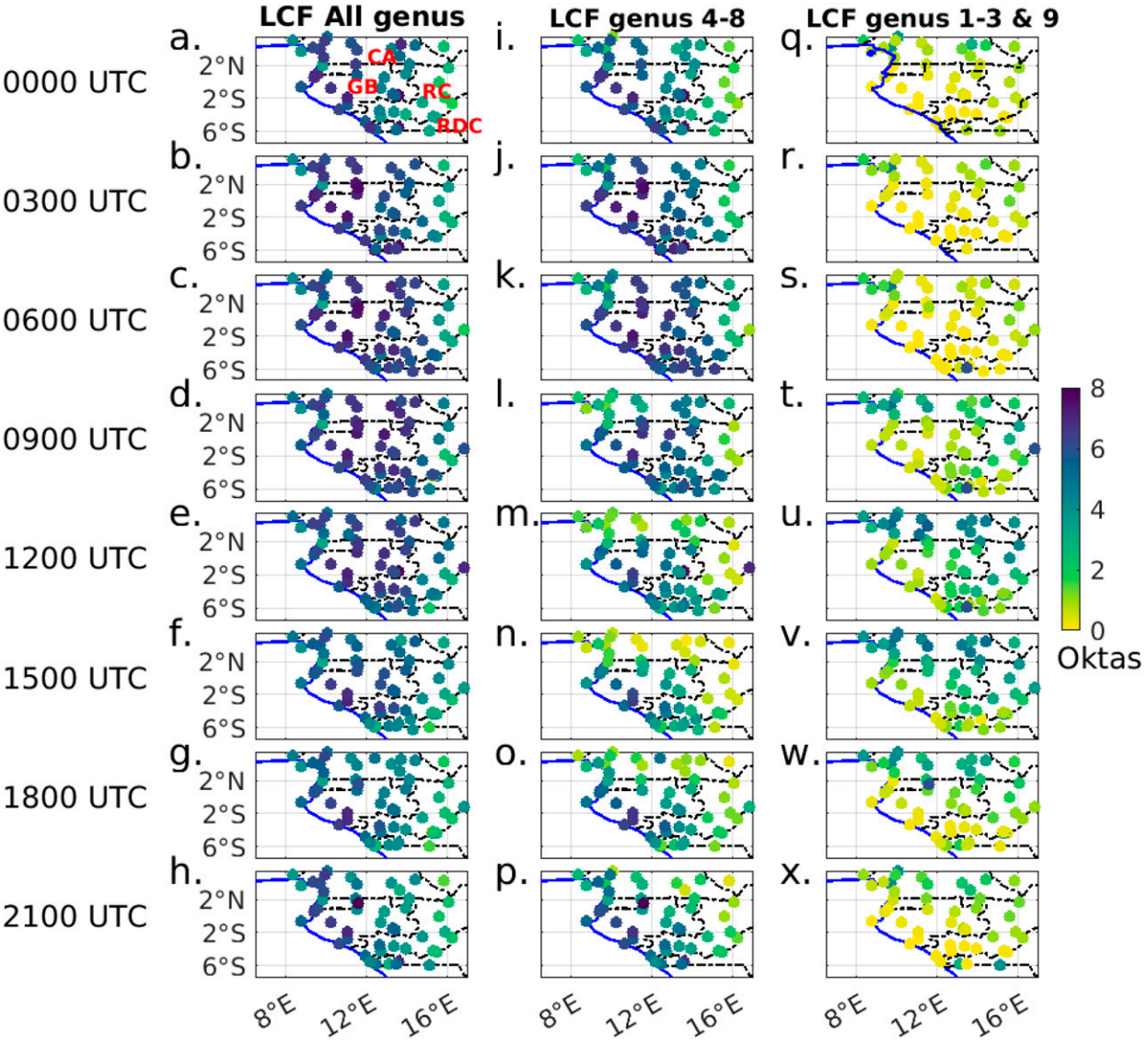

FIG. 4. JJAS (1971–2019) SYNOP low-level cloud fraction calculated from (a)–(h) all genera, (i)–(p) genera 4–8 only, and (q)–(x) genera 1–3 and 9 only per station and observation time.

1200 UTC, especially in Cameroon (Figs. 7n,d). Between 1200 and 1500 UTC LCOF decreases in the entire area, quite sharply with DMS (Figs. 7d,h), but stays high in western Gabon mainly in SAFNWC (Figs. 7c,g). The lower LCOF in the eastern part of the region in the afternoon suggests a sky clearing likely due to a transition from Sc to Cu shown in SYNOP data (Fig. 6). Between 1500 and 1800 UTC, corresponding to the period of the switch from the DMS to the NMS, the evolution of LCOF is different between SAFNWC (Figs. 7g,k) and the DMS/NMS microphysical scheme (Figs. 7h,l). While the LCOF continues to decrease during sunset in SAFNWC (a constant decrease according to Fig. S3), the LCOF starts to increase again in DMS/NMS, mainly in the coastal area. After 1800 UTC and throughout the night LCOF increases again in both products, but LCOF values in NMS (Figs. 7b,f,l,p) are almost twice those of SAFNWC (Figs. 7a,e,k,o). The increase of LCOF in NMS is again remarkable over the windward slopes and summit of the main mountain ranges and the coast of RC and RDC and has a wider expansion along the Chaillu Massif between 0000 and 0300 UTC (Figs. 7b,f).

The higher-level cloud occurrence frequency (HCOF) from SAFNWC and NMS/DMS is also shown in Fig. 7 (black dots) and points out the areas of higher uncertainty in the detection of low-level clouds from satellites. HCOF is larger in Cameroon, northern RC, and northern Gabon in both products and is increasing at night, reaching a 70% occurrence frequency in Cameroon in the NMS.

The twice-daily 2B-GEOPROF-lidar product does not allow to investigate the full diurnal cycle of the low-level cloud cover. However, it brings valuable information about clouds

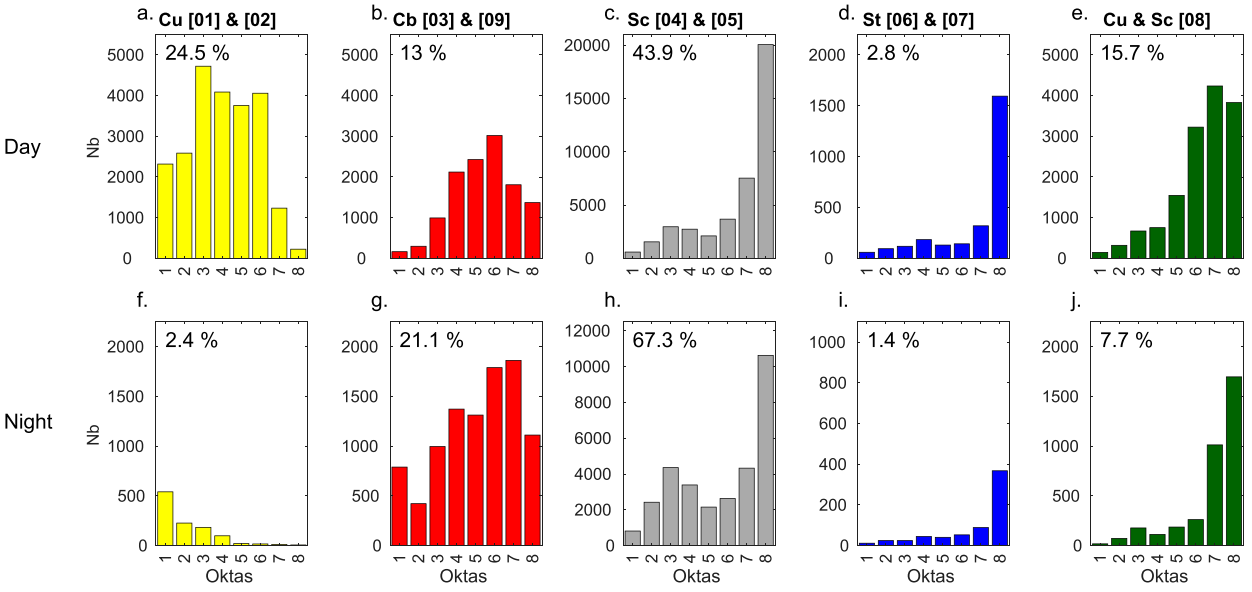

FIG. 5. JJAS (1971–2019) number of observations low-level cloud types from SYNOP per oktas from all stations for (a)–(e) daytime (0600–1500 UTC) and (f)–(j) nighttime (1800–0300 UTC). Percentages at the top give the frequency for each type over all SYNOP observation times.

heights and thickness for multiple cloud layers. Therefore, Fig. 8 displays climatologies for around 1230 and 0030 UTC of the vertical distribution (up to 20 km) of cloud occurrence frequency for six paths, as well as maps of LCOF (0–3000 m MSL). Around noon, the spatial variability of LCOF (Fig. 8d) is similar to the LCF (Fig. S4) and also similar to SAFNWC and DMS (Figs. 7c,d), namely, a widespread stratiform deck in Gabon, the western part of RC and southwestern Cameroon. The main difference compared to SAFNWC is a higher LCOF near the coast of Gabon in 2B-GEOPROF-lidar (Fig. 8d). The vertical distribution of clouds also shows more low-level clouds from the coastal plains to the west of the Chaillu Massif (Fig. 8b, 4°S–2°N). The other main feature is a higher base of low-level clouds over land (Figs. 8b,c) compared to the ocean (Fig. 8a), which might be due to the elevated terrain (red line in Figs. 8a–c). The low-level clouds are also thicker north of 2°S (up to 3000 m). In addition, multilayered higher clouds become more frequent toward northern areas (Figs. 8a–c) and mask the low-level clouds from the passive sensors on board satellites.

At midnight the LCOF from 2B-GEOPROF-lidar (Fig. 8f) shows generally less low-level clouds than at noon (Fig. 8d). A close inspection of Figs. 4i and 4m over central Gabon corroborates this finding: only later in the night and in the early morning the LCOF increases further and peaks in the diurnal cycle. In addition, the low-level clouds are more frequent near the coast compared to the plateau and their amount decreases inland toward the east (Fig. 8f), which is consistent with the results found with SAFNWC (Figs. 7a,e,o) and NMS (Figs. 7b,f,p). The clouds might be advected inland from the ocean, but because of the scarce twice-daily overflights the dynamics of the low-level clouds are difficult to estimate by 2B-GEOPROF-lidar. The vertical distribution of clouds confirms the expanded stratus deck to the west, i.e., on the windward slopes (Figs. 8e,g) while over the plateau farther east (Fig. 1), the low-level cloud occurrence is lower (Fig. 8h). The role of the topography is shown here clearer compared to daytime (Figs. 8a–c), likely due to the southwest–northeast orientation of 2B-GEOPROF-lidar path followed at night (Fig. 8f). In all nighttime paths, there are also larger amounts of high-level clouds over northern Gabon, northern RC, and Cameroon (Figs. 8e,g,h), consistent with SAFNWC and NMS (Figs. 7a,b).

The results suggest a widespread stratiform cloud deck in the morning that clears up in the afternoon mainly in the plateau east of Chaillu massif and Cristal mountains. However, some inconsistencies between products have been found mainly due to the inability of SAFNWC to detect low-level clouds at night. The multilayered cloud cover mostly present in northern Gabon and southern Cameroon at night as seen from 2B-GEOPROF-lidar, may partly explain the lower number of low-level clouds detected with SAFNWC and NMS there compared to SYNOP observations (section 3a). The aim of the next section is to thoroughly compare SYNOP observations and satellite data.

c. *Comparison of satellite and station observations*

In this section, LCF from satellites and from SYNOP observations are compared. The average LCF in the entire area is very different between a LCF calculated with all SYNOP genus or excluding cumuliform low-level clouds (genera 4–8 only). During the day (1200–1500 UTC) the LCF excluding cumuliform clouds is lower by approximately 2 oktas. Focusing on the latter, the highest level (more than 5 oktas) is reached at 0600 UTC (Fig. 9a). The LCF decreases during the day to reach a minimum at 1500 UTC (3 oktas). The diurnal cycle of LCF from satellites is similar between SAFNWC and

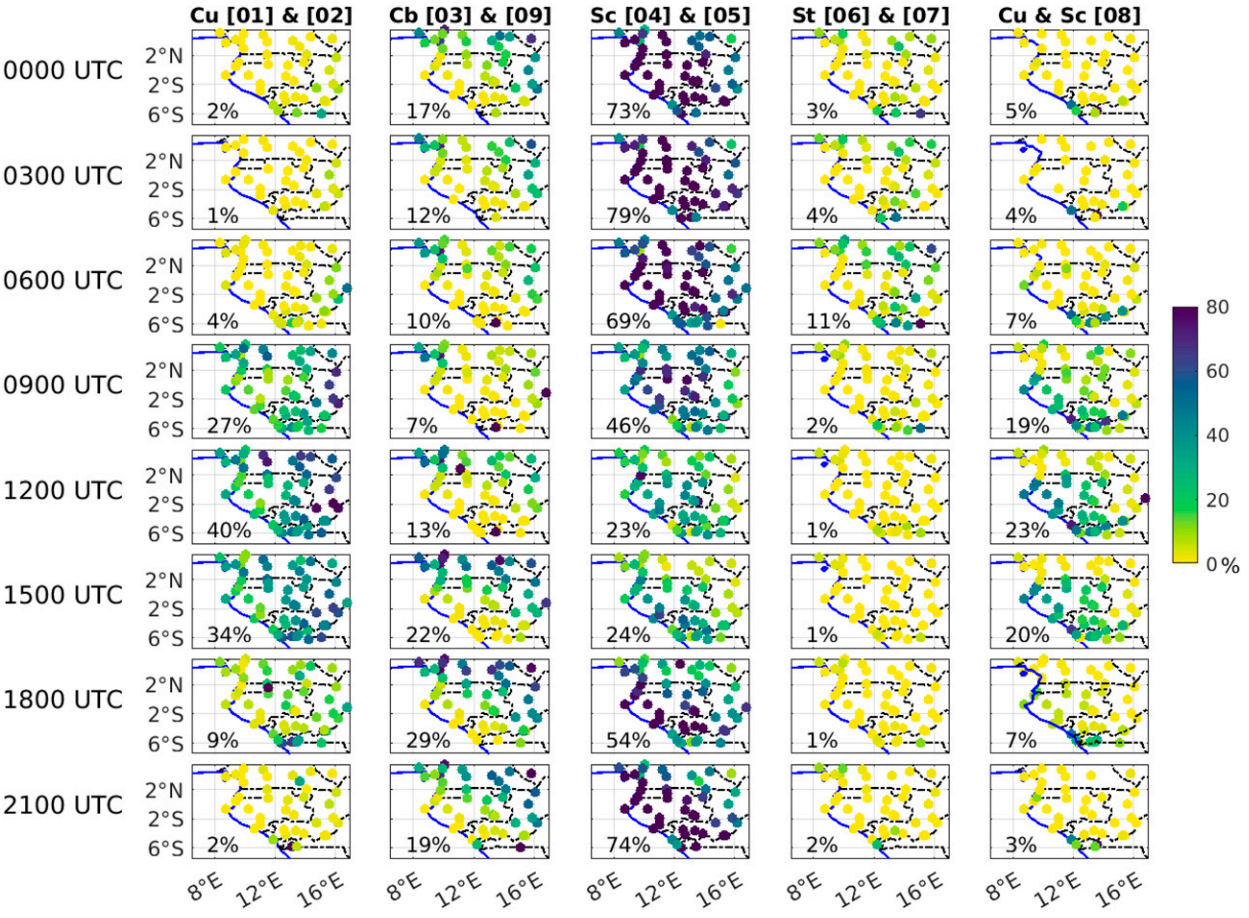

FIG. 6. JJAS (1971–2019) SYNOP cloud genus occurrence frequency per station and observation time. For each panel, the number at the bottom left shows at each observation time the average fraction of the given cloud genus.

DMS during the day (0600–1500 UTC, Fig. 9a) with a peak at midday. In the early morning (0600 UTC) when the solar angle is low, both satellite products underestimate the SYNOP observations because of low illumination. LCF from satellites overestimates SYNOP observations at midday (1200 UTC) when cumuliform clouds are not counted in SYNOP observations (Fig. 9a). In the afternoon, satellite products show a decrease of LCF, reaching a level close to SYNOP observations (around 3 oktas at 1500 UTC). At night (1800–0300 UTC), LCF from SAFNWC shows a large underestimation (2 oktas) compared to SYNOP observations while NMS show closer results to SYNOP observations (Fig. 9a).

The bias between satellite datasets and SYNOP observations is highly dependent on the region (Figs. 9b–q). At 0600 UTC the underestimation of LCF from satellites is larger in western RC and western Gabon (Figs. 9j,k). During the day LCF starts to be overestimated mainly in the northeast part of RC (Figs. 9n,o,d,e,h,i), where the cumuliform clouds are more prevalent (Fig. 6). At night (1800–0300 UTC) less stations have a sufficient amount of data for the analysis (mainly in central Gabon), which degrades the accuracy of the results, but regional variability is still appearing. In western RC, a large underestimation appears in SAFNWC (Figs. 9l,p,b,f) while NMS shows a slight overestimation (Figs. 9m,q,c,g). Over coastal Gabon, LCF is underestimated by a similar amplitude in both products. The bias in terms of LCOF was also calculated (Fig. S5) and show similar results. In addition, a statistical analysis (Receiver Operating Characteristic curve and a Heidke skill score) comparing SYNOP observations and satellite data is shown in Fig. S6.

The occurrence of low-level cloud genus from SYNOP observations and the occurrence of low-level cloud types from satellite data are finally compared to investigate how the satellites detect the different cloud genus. Figure 10 displays the diurnal cycle of the frequency of low-level cloud genus as observed at the stations (colored bars) for each satellite cloud type (individual panels).

Very low and low clouds together are the most frequent SAFNWC cloud types during the day (black line, Fig. 10) and are mostly detected when nonconvective clouds (stratocumulus) are observed from the ground (gray shade, Figs. 10b,c). Cloud-free is detected more frequently at night and early morning (1800–0600 UTC) and corresponds also mostly to observed stratocumulus (Fig. 10a), confirming that a large part of stratiform clouds observed from the ground are not well detected

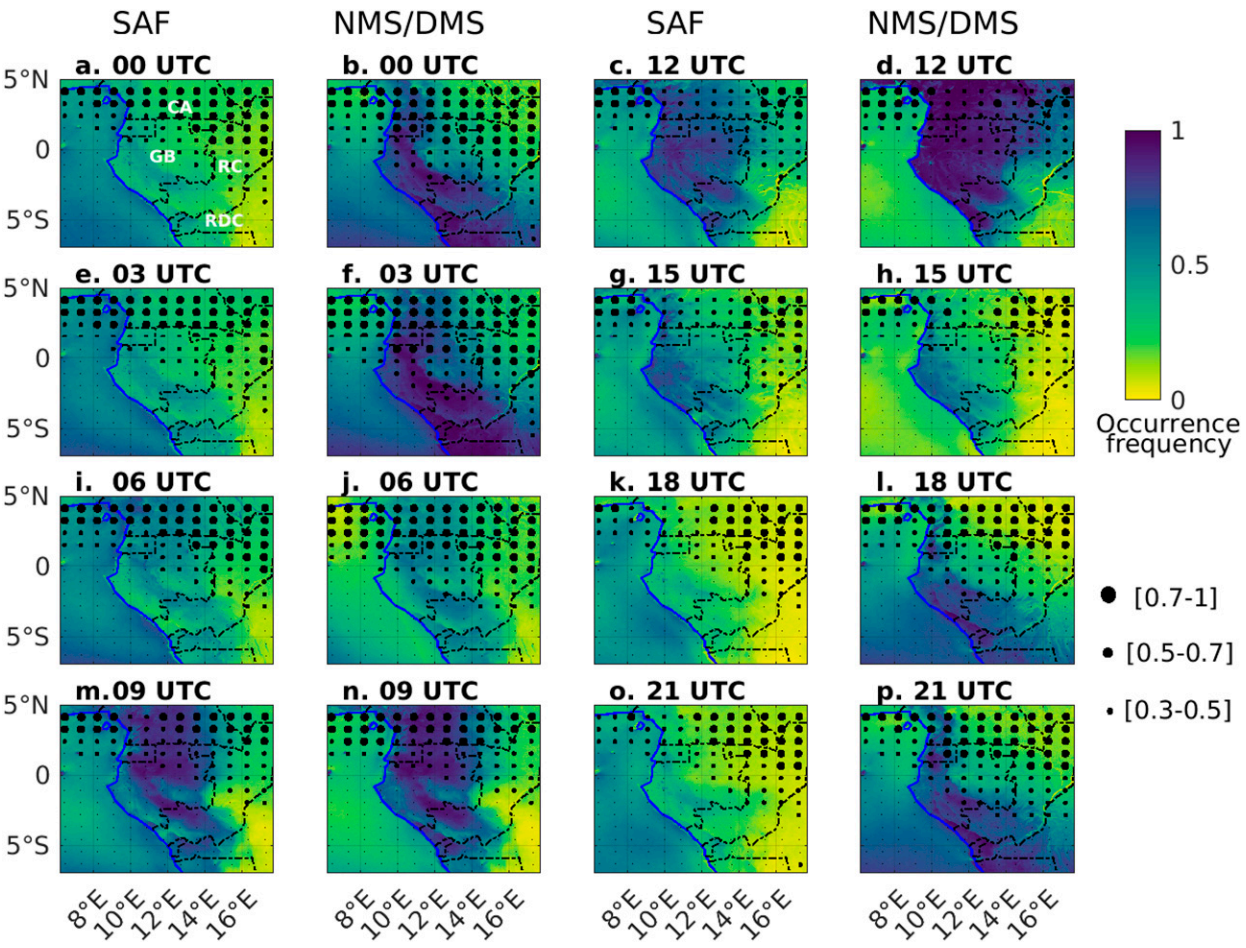

FIG. 7. JJAS low-level clouds occurrence frequency (shading) and high clouds (dots) from SAFNWC and NMS/DMS for the eight observation times available at the analyzed stations in the period 2008–19.

by SAFNWC at night. As previously discussed in van der Linden et al. (2015), this is partly related to small temperature differences between low-level clouds and the ground, making it difficult to detect low-level clouds using IR brightness temperature. In addition, high water vapor content in low levels makes it difficult to adjust thresholds to detect cloudy pixels. During the day (0900–1500 UTC), cumulus clouds prevail when no cloud is detected in satellites (Fig. 10a). Cumulus clouds are also frequent in the fractional type (Fig. 10f) due to the fractional characteristic of cumulus. Cumulus covers only a part of the sky (Fig. 5), so they are likely to be classified as cloud-free in SAFNWC (Fig. 10a). The type "high semi-transparent" is also well represented and occurs steadily during the day at a frequency between 15% and 20% (black line, Fig. 10g). These high clouds from SAFNWC are associated with a significant number of stratocumulus in SYNOP observations (Fig. 10g) showing that the high clouds are likely hiding part of the stratocumulus situated underneath and seen from the ground.

The three DMS/NMS types include low-level clouds (Microphysical Scheme low-level cloud cover, MS lcc), higher level clouds (Microphysical Scheme higher-level cloud cover, MS hcc), and cloud-free (MS cloud-free). These types have more intertypes similarities than SAFNWC in terms of partition of SYNOP cloud genus. The main difference among DMS/NMS types is a slightly higher proportion of stratocumulus in the low-level cloud type and a higher proportion of cumulonimbus in the cloud-free type (Figs. 10h–j).

Overall, the comparison between SYNOP observations and satellite data described in this section suggests clearly that NMS is more realistic than SAFNWC in detecting the low-level clouds at nighttime. During the day, SAFNWC shows an LCF bias similar to DMS (Fig. 9) but shows a higher proportion of stratocumulus detected as low clouds (Fig. 10).

d. Spatial variability in the diurnal cycle of low-level cloud cover

The previous section has shown large differences between SYNOP observations and satellite products in absolute values of low-level cloud cover. Quantifying the change of low-level cloud cover between successive observation times may therefore better reveal the spatial consistencies of diurnal cycles in the different products. In this section, the evolution of JJAS

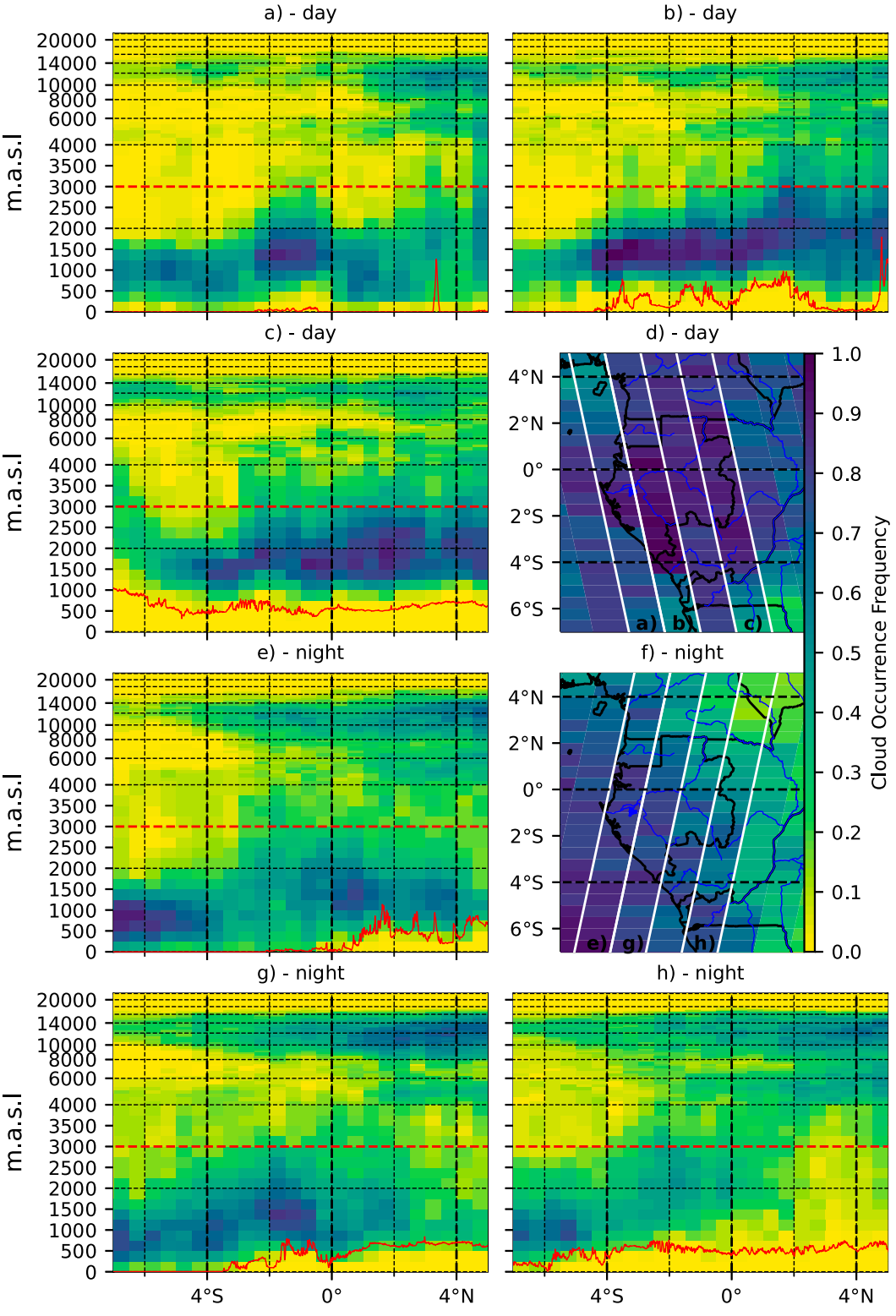

FIG. 8. JJAS vertical cloud occurrence frequency from 2B-GEOPROF-lidar along three paths at (a)–(c) 1230 and (e),(g),(h) 0030 UTC for the period 2006–17 during the day and 2006–10 during the night. The red line is the topography. The LCOF calculated in each swath between the ground level and 3000 m MSL (horizontal red dotted line) are shown at (d) 1230 and (f) 0030 UTC.

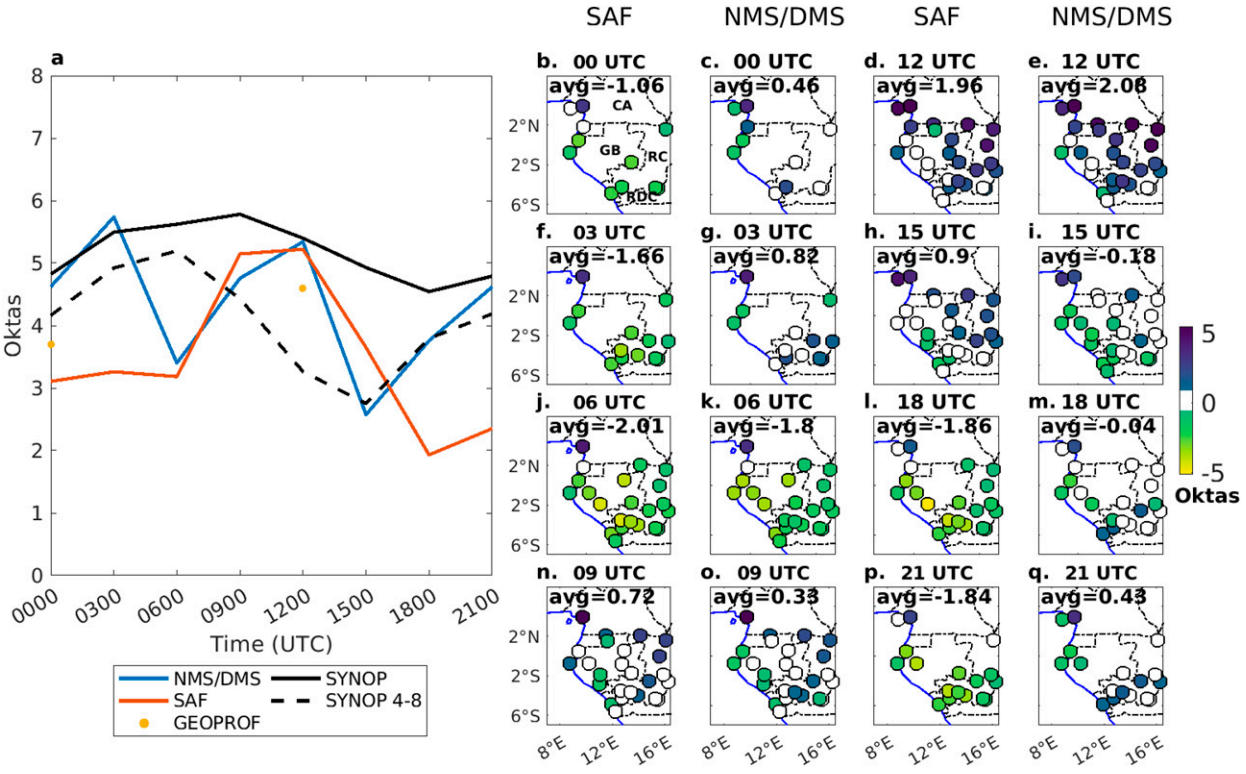

FIG. 9. (a) Spatially averaged diurnal cycle of LCF from SAFNWC, NMS (1800–0300 UTC), DMS (0600–1500 UTC), and SYNOP observations (all genera and genera 4–8 only). All stations have the same weight regardless of their sample size. (b)–(q) Maps of the mean bias (in oktas) between LCF from SAFNWC or NMS/DMS and SYNOP observations (genera 4–8) for the period JJAS 2008–19. "Avg" represents the average bias from all stations. The stations with less than 10% of available data have been removed from the analysis for each observation time.

LCOF between successive observation times in the period 2008–19 using NMS, SAFNWC, and SYNOP observations is investigated (Fig. 11). NMS is used for nighttime (Figs. 11a,b) and SAFNWC for daytime (Figs. 11c,d) because these products are more reliable in these respective periods, as shown in the previous section. The times 1800 and 0600 UTC have been removed from this analysis since low-level clouds at these times are not well captured by the satellites (Fig. 9) due to twilight conditions.

The results from SYNOP observations show that LCOF increases in the evening, starting from western Gabon and western Cameroon, and spreading to the east (Figs. 11a,b). The results from the NMS show a similar spatial variability before midnight with the largest LCOF increase in the Cristal Mountains in northern Gabon and in south-central Cameroon (Fig. 11a). After midnight and until 0300 UTC, the cloudiness keeps increasing in these regions, but also increases farther east (Fig. 11b).

During the day, the SYNOP observations show generally a decrease of low-level cloud cover (green and yellow circles in Fig. 11d), but some stations show a very small change in LCOF, mainly in the central and northern part of RC (blue and white circles in Figs. 11c,d), most likely due to the development of low-level cumulus clouds (Fig. 6). A stable LCOF is also evident in the coastal hinterlands on the windward side of the Cristal and Chaillu mountain ranges (Figs. 11c,d). The spatial variability of low-level cloud cover diurnal evolution from SAFNWC is moderately consistent with the SYNOP observations: it shows an increase in LCOF in the morning (0900–1200 UTC) in the central and northern part of RC and the coastal hinterlands, in regions of very low change of LCOF according to SYNOP observations (Fig. 11c). Between 1200 and 1500 UTC results from SAFNWC show a general decrease of LCOF (green and yellow shades in Fig. 11d) except for the coastal hinterlands (blue and white shades in Fig. 11d).

To investigate the difference of mean diurnal cycle between different regions of the area, stations with at least 10% of available data for each observation between 0300 and 2100 UTC have been identified (Fig. 11e) and grouped according to their geographical locations. The average SYNOP observations and SAFNWC LCOF diurnal cycle for these stations have been calculated and plotted on Figs. 11f and 11g. Looking at the SYNOP data, the coastal stations, including Pointe-Noire, Mayumba, Port-Gentil, and Libreville (in red) show very high LCOF at night (80%), slightly decreasing during the day reaching 60% at 1500 UTC (Fig. 11f). The windward slopes of the Chaillu Mountains represented by the stations Dolisie, Makabana, Tchibanga, Mouila, and Lambarene (orange, cf. Fig. 1) are the cloudiest and show a steady LCOF around 70%–80%. Stations

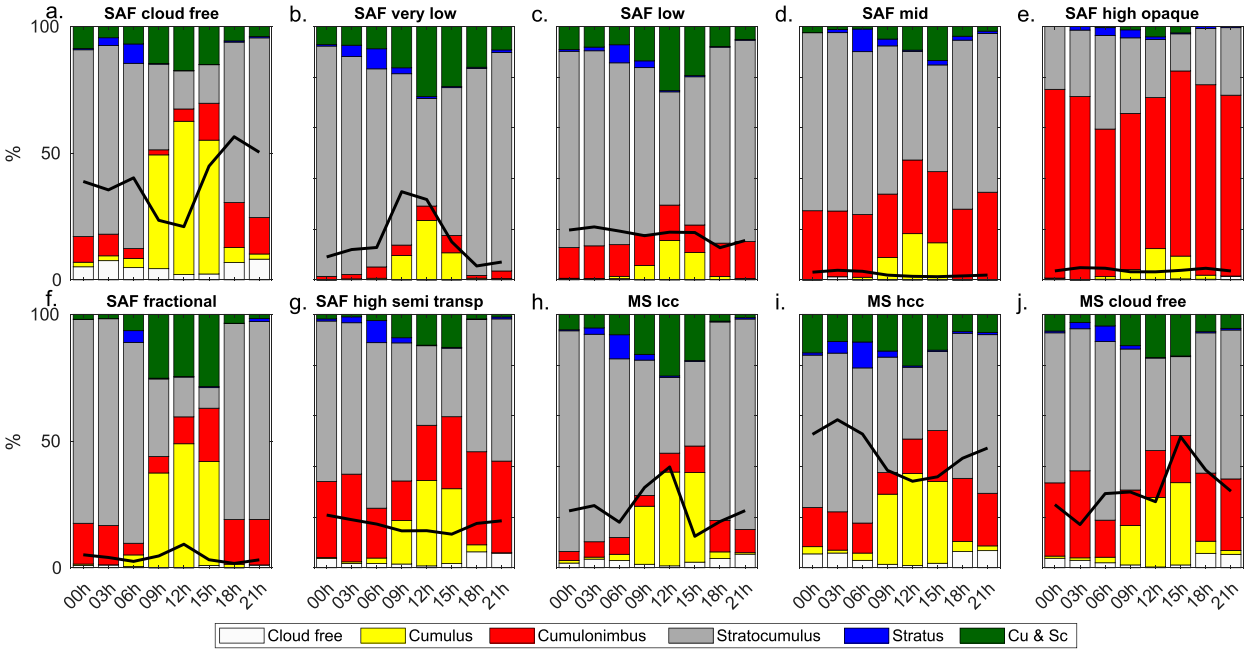

FIG. 10. All stations diurnal partition of the SYNOP low-level cloud genus (colored bars) in the seven SAFNWC ("SAF" panels) and the three NMS/DMS ("MS" panels) cloud types for the period JJAS 2008–19. The NMS was used from 1800 to 0300 UTC and the DMS from 0600 to 1500 UTC. Black line is the frequency of each SAFNWC or NMS/DMS cloud type relative to the number of all available SYNOP observations. The stations with less than 10% of available data have been removed from the analysis for each observation time.

in the plateau region, including Mouyondzi, Sibiti, Franceville, Lastoursville, Makokou, and Mitzic (green), show a LCOF peaking at 80% around 0600 UTC then decreasing in the afternoon to less than 50%. Farther east in the region including Brazzaville, Kinshasa-Ndjili, Djambala, and Souanké (blue, leeward slopes of plateau) the LCOF is generally lower and shows a stronger diurnal cycle with LCOF varying between 70% in the morning and 25% in the afternoon (Fig. 11f). Taking the grid point corresponding to each station, SAFNWC during the day (0600–1500 UTC) and NMS at night (1800–0300 UTC) the spatial variability of diurnal cycle is similar to SYNOP observations data (similar ranking of the groups of stations; Fig. 11g). During the day, we observe an eastward gradient, with a higher cloud occurrence frequency in the windward slopes and lower cloud cover toward the inland region (Fig. 11g). At night (0000–0300 UTC) the difference of low-level cloud cover between the windward slopes and the inland regions is reduced, similarly to SYNOP observations (Figs. 11f,g). Inconsistencies between SYNOP observations and satellites include a large underestimation of LCOF at 0600 UTC (see also Fig. 9) and a clear underestimation at the coastal stations due to less low-level cloud over the ocean in SAFNWC.

The reduced low-level cloud cover over the plateau in the afternoon has been previously associated to the topography favoring a foehn effect (Dommo et al. 2018). The afternoon clearing occurring on the plateau may also be associated with shortwave heating and stronger convection due to elevated terrain. The development of cumulus in eastern Gabon and central RC supports this statement (Fig. 6). The June–July daytime clearing of the low-level stratus in southern Benin during the "convective phase," as described in the conceptual model of Lohou et al. (2020), provides a potential mechanism in this regard. However, a clear distinction to the Benin site is the presence of a lush rain forest in Gabon and thus plant transpiration might be of larger importance. After sunset, the LW cooling of the ground and later of the cloud top might promote the formation of the clouds.

On the windward slopes of southern Cameroon, Equatorial Guinea, Gabon, and RC, the apparent increase of low-level cloud cover during the morning in the satellites, while collocated stations do not actually show any LCF increase (Figs. 7 and 11c), may be associated with a thickening of the boundary layer height that makes the low-level clouds "visible" to the satellite. Early in the morning, the low-level cloud top temperature may not be significantly distinct from the ground temperature, such that the low-level clouds can easily be misclassified as cloud-free by the satellite's algorithm. This result suggests a persistence of low-level clouds as shown in the SYNOP observations (Fig. 11f) more than a real increase in low-level cloud cover. To the east of the coastal plains, at the western flank of the low mountain ranges, upslope winds will support the persistence of clouds. While for Southern West Africa, it was found that advection of low-level marine stratus onto land plays an inferior role to the extent of the land-based stratus (Lohou et al. 2020), this may be a contributor south of Port-Gentil where low-level offshore clouds are frequent and widespread (Fig. 7).

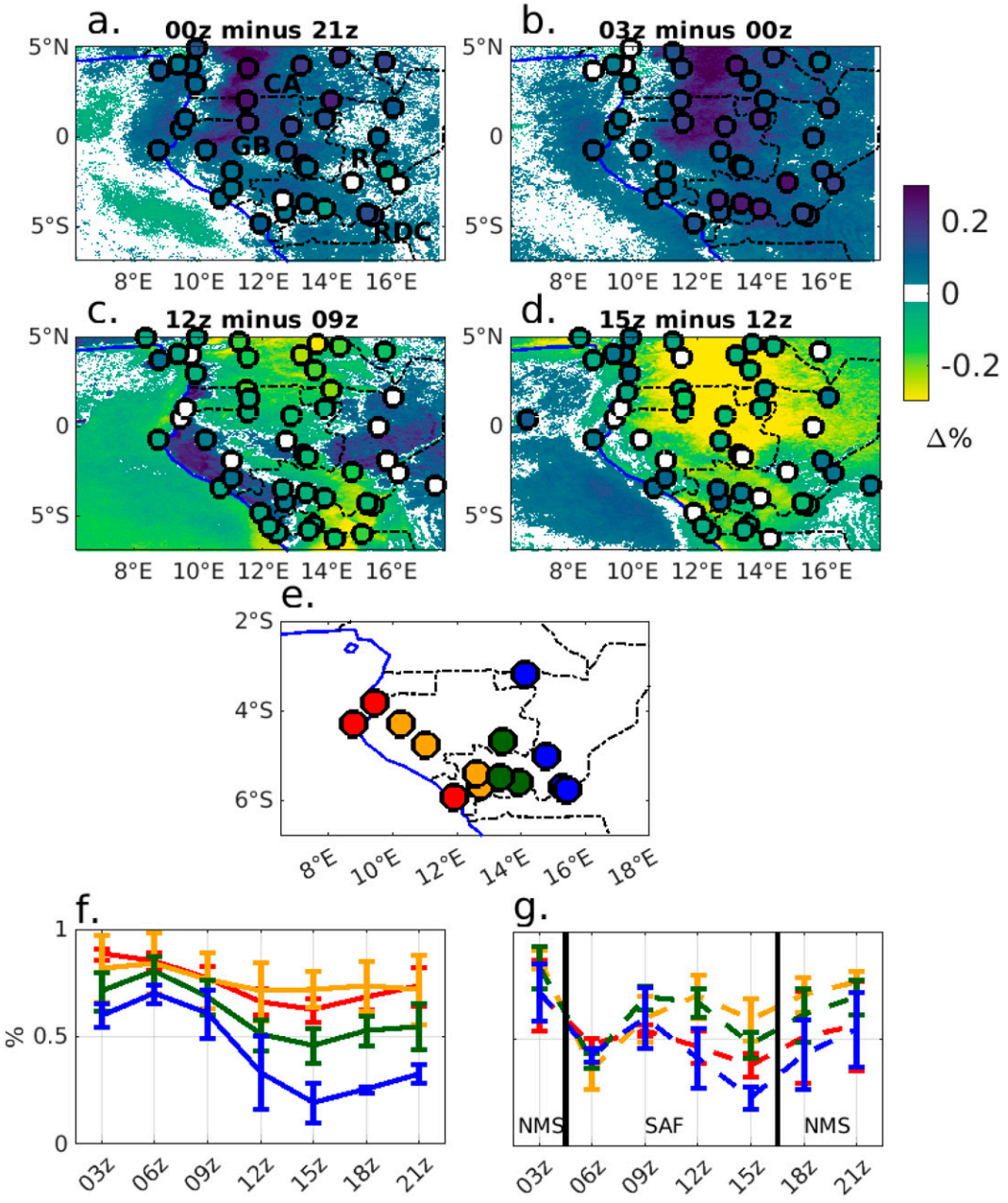

FIG. 11. Change of LCOF compared to the previous observation time for (a),(b) NMS at nighttime and (c),(d) SAFNWC at daytime for the period JJAS 2008–19. The circles are the in situ observed change of LCOF in the period JJAS 1971–2019 for stations with less than 10% of missing data. (e) Location of the stations investigated in (f) and (g). (f),(g) Average and standard deviation of LCOF from (f) SYNOP observations and (g) satellites at the coast (red), on the windward slopes and coastal plains (orange), on the plateau (green), and leeward slopes of Congo basin (blue). The vertical lines in (g) delineate the hours when LCOF is calculated from SAFNWC (0600–1500 UTC) and from NMS (1800–0300 UTC).

Stations directly at the coast, like Port-Gentil at Cape Lopez and Pointe-Noire, but to a lesser extent Libreville (red stations in Fig. 11e), exhibit a decrease of low-level cloud cover in the morning, suggesting a frequent land–sea breeze, even during the cloudy dry season. It is interesting to note that the coastal upwelling develops south of Port-Gentil (Herbert and Bourlès 2018). Thus, the larger ocean–land temperature contrasts at Pointe-Noire and the "cape location" of Port-Gentil may favor a decrease of the low-level cloud cover in the morning due to a sea breeze.

4. Summary and discussion

In this study, a dataset of SYNOP observations of low cloud fraction and low cloud genus of unprecedented length (1971–2019) and completeness has been compiled for western equatorial Africa. It has been used to provide a climatology of low-level clouds and to evaluate satellite cloud products, namely, SAFNWC and NMS/DMS for the common period JJAS 2008–19. SAFNWC, NMS, and DMS products are based on the MSG SEVIRI multichannel radiometer and thus have a high spatial (3 km × 3 km) and temporal (15 min) resolution. 2B-GEOPROF-lidar which is based on the *CloudSat*/CPR and *CALIPSO*/CALIOP instruments, and has a low sampling rate (two overflights per day and a return period of 16 days for the same swath), was also considered and reveals an exceptional insight into multilayered cloud cover.

Our evaluations of the satellite products (Fig. 9) underscore the previously known deficiencies of SAFNWC at detecting low-level clouds at night in tropical Africa (van der Linden et al. 2015; Dommo et al. 2018). The lower skill of SAFNWC compared to NMS at night is demonstrated by the proportion of undetected low-level clouds (all genera): in NMS only ~25% (Fig. 10h) of the SYNOP low-level clouds are classified in the cloud-free category (among which a significant number of cumulonimbus), whereas in SAFNWC this number is above 40% (Figs. 10b,c) and comprises mainly stratocumulus. Thresholds used in the NMS algorithm are probably more efficient to capture low-level clouds, especially in case of a small contrast between the ground and the cloud top temperature. A negative bias at night in SAFNWC due to such a small contrast has previously been reported (van der Linden et al. 2015). Therefore, the use of the NMS, adapted for tropical conditions (Schrage and Fink 2012) is also recommended for western equatorial Africa. Consequently, the concatenation of SAFNWC for daylight hours (0600–1500 UTC) and NMS for nighttime (1800–0300 UTC) hours yields the most realistic diurnal cycle compared to SYNOP observations, although caution should be exerted around sunset and sunrise as both products show large biases. Our study clearly improves on the results by Dommo et al. (2018) as this former study shows a maximum of low-level cloud cover in late morning in all parts of western equatorial Africa, whereas low-level cloud cover (excluding cumuliform clouds) peaks at late night/early morning.

The satellite products SAFNWC and NMS were together able to produce a similar spatial variability of low-level clouds diurnal cycle compared to SYNOP observations. Mostly, over the windward slopes of the Cristal and Chaillu Mountains (Fig. 1), there is more low-level clouds all day, while the plateau regions are characterized by a larger amplitude in the diurnal cycle with higher LCOF in the morning, a decrease of LCOF (clearing) in the afternoon, and low-level clouds that reform late at night (Figs. 7 and 11). However, frequent higher clouds, well captured in the 2B-GEOPROF-lidar vertical profiles (Fig. 8), render the results more uncertain in the northern part of the study region (i.e., south Cameroon, Fig. 7), and partly explains the larger underestimation of low-level clouds by SAFNWC and the microphysical schemes compared to SYNOP observations in this region.

Despite uncertainties in both eye observations of clouds at stations and satellite cloud products, the present study yields the most complete low-level cloud climatology for western equatorial Africa to date and can provide a basis for further investigations on climate change aspects of low-level clouds. First, this paper points to the observational and satellite products that can be used for validating climate models over the historical period for the region. Second, it documents the mean diurnal evolution of the low-level cloud cover and the spatial variability of cloud fraction and frequency of occurrence. If models show a good performance at reproducing these key characteristics over the historical period, then one should have some confidence to use them for exploring the medium to long-term future evolution of the low-level cloud cover. Coupled and forced CMIP6 models have still large deficiencies in simulating the low-level oceanic and continental clouds in the region (Camberlin et al. 2023), but convection-permitting model simulations, including sensitivity studies, should be suitable to shed more light on the physical processes involved in the genesis and lysis of the low-level clouds.

Acknowledgments. The authors thank the reviewers for their time spent on the manuscript and their valuable comments. We also thank the AERIS/ICARE data center (http://icare.univ-lille1.fr/) for providing access to the SAFNWC CT data used in this study. This study was part of the project DYVALOCCA (https://dyvalocca.osug.fr/) funded by ANR and DFG under Contract ANR-19-CE01-0021 and DFG FI 786/5-1.

Data availability statement. The datasets used to create the concatenated SYNOP dataset are from different sources: EECRA is available at https://rda.ucar.edu/datasets/ds292.2/#access. ISD is from https://www.ncei.noaa.gov/products/land-based-station/integrated-surface-database. MIDAS is from https://catalogue.ceda.ac.uk/uuid/220a65615218d5c9cc9e4785a3234bd0. SAFNWC is available upon request from the AERIS/ICARE data center (http://icare.univ-lille1.fr/). The raw data from the Meteosat Second Generation used to construct DMS, NMS, and SAFNWC data are available here: https://data.eumetsat.int/product/EO:EUM:DAT:MSG:HRSEVIRI#. 2B-GEOPROF-LIDAR is available here: 2B-GEOPROF-LIDAR | CloudSat DPC (colostate.edu). The concatenated SYNOP observations dataset is freely available (DOI: 10.5445/IR/1000150635). The low cloud occurrence frequency and low cloud fraction from SAFNWC, NMS/DMS and 2B-GEOPROF-LIDAR produced in this study are available upon request.

REFERENCES

Adebiyi, A. A., and P. Zuidema, 2018: Low cloud cover sensitivity to biomass-burning aerosols and meteorology over the southeast Atlantic. *J. Climate*, **31**, 4329–4346, https://doi.org/10.1175/JCLI-D-17-0406.1.

Aellig, R., V. Moron, and P. Camberlin, 2022: Cloud observing data of 85 stations in western Central Africa. KIT, accessed 23 September 2022, https://doi.org/10.5445/IR/1000150635.

Alexandersson, H., and A. Moberg, 1997: Homogenization of Swedish temperature data. Part I: Homogeneity test for linear trends. *Int. J. Climatol.*, **17**, 25–34, https://doi.org/10.1002/(SICI)1097-0088(199701)17:1<25::AID-JOC103>3.0.CO;2-J.

Andersen, H., and J. Cermak, 2018: First fully diurnal fog and low cloud satellite detection reveals life cycle in the Namib. *Atmos. Meas. Tech.*, **11**, 5461–5470, https://doi.org/10.5194/amt-11-5461-2018.

——, ——, I. Solodovnik, L. Lelli, and R. Vogt, 2019: Spatiotemporal dynamics of fog and low clouds in the Namib unveiled with ground- and space-based observations. *Atmos. Chem. Phys.*, **19**, 4383–4392, https://doi.org/10.5194/acp-19-4383-2019.

——, ——, J. Fuchs, P. Knippertz, M. Gaetani, J. Quinting, S. Sippel, and R. Vogt, 2020: Synoptic-scale controls of fog and low-cloud variability in the Namib Desert. *Atmos. Chem. Phys.*, **20**, 3415–3438, https://doi.org/10.5194/acp-20-3415-2020.

Bayon, G., and Coauthors, 2019: The roles of climate and human land-use in the late Holocene rainforest crisis of Central Africa. *Earth Planet. Sci. Lett.*, **505**, 30–41, https://doi.org/10.1016/j.epsl.2018.10.016.

Berry, Z. C., and G. R. Goldsmith, 2020: Diffuse light and wetting differentially affect tropical tree leaf photosynthesis. *New Phytol.*, **225**, 143–153, https://doi.org/10.1111/nph.16121.

Burnett, M. W., G. R. Quetin, and A. G. Konings, 2020: Data-driven estimates of evapotranspiration and its controls in the Congo Basin. *Hydrol. Earth Syst. Sci.*, **24**, 4189–4211, https://doi.org/10.5194/hess-24-4189-2020.

Bush, E. R., and Coauthors, 2020: Rare ground data confirm significant warming and drying in western equatorial Africa. *PeerJ*, **8**, e8732, https://doi.org/10.7717/peerj.8732.

Camberlin, P., and Coauthors, 2023: The representation of dry-season low-level clouds over western equatorial Africa in reanalyses and historical CMIP6 simulations. *Climate Dyn.*, https://doi.org/10.1007/s00382-023-06714-w, in press.

Danielson, J. J., and D. B. Gesch, 2011: Global multi-resolution terrain elevation data 2010 (GMTED2010). USGS Open-File Rep. 2011-1073, 34 pp., https://pubs.usgs.gov/of/2011/1073/pdf/of2011-1073.pdf.

Dee, D. P., and Coauthors, 2011: The ERA-Interim reanalysis: Configuration and performance of the data assimilation system. *Quart. J. Roy. Meteor. Soc.*, **137**, 553–597, https://doi.org/10.1002/qj.828.

Derrien, M., and H. Le Gléau, 2005: MSG/SEVIRI cloud mask and type from SAFNWC. *Int. J. Remote Sens.*, **26**, 4707–4732, https://doi.org/10.1080/01431160500166128.

——, H. L. Gleau, and P. Fernandez, 2013: Algorithm theoretical basis document for "Cloud Products" (CMa-PGE01 v3.2, CT-PGE02 v2.2 & CTTH-PGE03 v2.2). NWC SAF, 87 pp., https://www.nwcsaf.org/AemetWebContents/ScientificDocumentation/Documentation/MSG/SAF-NWC-CDOP2-MFL-SCI-ATBD-01_v3.2.1.pdf.

Dommo, A., N. Philippon, D. A. Vondou, G. Sèze, and R. Eastman, 2018: The June–September low cloud cover in western Central Africa: Mean spatial distribution and diurnal evolution, and associated atmospheric dynamics. *J. Climate*, **31**, 9585–9603, https://doi.org/10.1175/JCLI-D-17-0082.1.

Eastman, R., and S. G. Warren, 2014: Diurnal cycles of cumulus, cumulonimbus, stratus, stratocumulus, and fog from surface observations over land and ocean. *J. Climate*, **27**, 2386–2404, https://doi.org/10.1175/JCLI-D-13-00352.1.

EUMeTrain, 2017: Composite Image Quick Guide. Accessed 14 April 2022, https://resources.eumetrain.org/rgb_quick_guides/index.html.

Fleury, L., and Coauthors, 2011: AMMA information system: An efficient cross-disciplinary tool and a legacy for forthcoming projects. *Atmos. Sci. Lett.*, **12**, 149–154, https://doi.org/10.1002/asl.303.

Fuchs, J., J. Cermak, and H. Andersen, 2018: Building a cloud in the southeast Atlantic: Understanding low-cloud controls based on satellite observations with machine learning. *Atmos. Chem. Phys.*, **18**, 16 537–16 552, https://doi.org/10.5194/acp-18-16537-2018.

Geleyn, J.-F., and A. Hollingsworth, 1979: An economical analytical method for the computation of the interaction between scattering and line absorption of radiation. *Beitr. Phys. Atmos.*, **52**, 1–16.

Goldsmith, G. R., N. J. Matzke, and T. E. Dawson, 2013: The incidence and implications of clouds for cloud forest plant water relations. *Ecol. Lett.*, **16**, 307–314, https://doi.org/10.1111/ele.12039.

Hahn, C., S. Warren, and R. Eastman, 1999: Extended edited synoptic cloud reports from ships and land stations over the globe, 1952-2009 (NDP-026C). ORNL, accessed 15 February 2020, https://doi.org/10.3334/CDIAC/cli.ndp026c.

Herbert, G., and B. Bourlès, 2018: Impact of intraseasonal wind bursts on sea surface temperature variability in the far eastern tropical Atlantic Ocean during boreal spring 2005 and 2006: Focus on the mid-May 2005 event. *Ocean Sci.*, **14**, 849–869, https://doi.org/10.5194/os-14-849-2018.

Hu, Z.-Z., B. Huang, and K. Pegion, 2008: Low cloud errors over the southeastern Atlantic in the NCEP CFS and their association with lower-tropospheric stability and air-sea interaction. *J. Geophys. Res.*, **113**, D12114, https://doi.org/10.1029/2007JD009514.

Kalthoff, N., and Coauthors, 2018: An overview of the diurnal cycle of the atmospheric boundary layer during the West African monsoon season: Results from the 2016 observational campaign. *Atmos. Chem. Phys.*, **18**, 2913–2928, https://doi.org/10.5194/acp-18-2913-2018.

Karger, D. N., M. Kessler, M. Lehnert, and W. Jetz, 2021: Limited protection and ongoing loss of tropical cloud forest biodiversity and ecosystems worldwide. *Nat. Ecol. Evol.*, **5**, 854–862, https://doi.org/10.1038/s41559-021-01450-y.

Knippertz, P., A. H. Fink, R. Schuster, J. Trentmann, J. M. Schrage, and C. Yorke, 2011: Ultra-low clouds over the southern West African monsoon region. *Geophys. Res. Lett.*, **38**, L21808, https://doi.org/10.1029/2011GL049278.

——, and Coauthors, 2015: The DACCIWA project: Dynamics–aerosol–chemistry–cloud interactions in West Africa. *Bull. Amer. Meteor. Soc.*, **96**, 1451–1460, https://doi.org/10.1175/BAMS-D-14-00108.1.

Lensky, I. M., and D. Rosenfeld, 2008: Clouds-Aerosols-Precipitation Satellite Analysis Tool (CAPSAT). *Atmos. Chem. Phys.*, **8**, 6739–6753, https://doi.org/10.5194/acp-8-6739-2008.

Lohou, F., N. Kalthoff, B. Adler, K. Babić, C. Dione, M. Lothon, X. Pedruzo-Bagazgoitia, and M. Zouzoua, 2020: Conceptual model of diurnal cycle of low-level stratiform clouds over southern West Africa. *Atmos. Chem. Phys.*, **20**, 2263–2275, https://doi.org/10.5194/acp-20-2263-2020.

Mace, G. G., and Q. Zhang, 2014: The CloudSat radar-lidar geometrical profile product (RL-GeoProf): Updates, improvements, and selected results. *J. Geophys. Res. Atmos.*, **119**, 9441–9462, https://doi.org/10.1002/2013JD021374.

——, ——, M. Vaughan, R. Marchand, G. Stephens, C. Trepte, and D. Winker, 2009: A description of hydrometeor layer occurrence statistics derived from the first year of merged Cloudsat and CALIPSO data. *J. Geophys. Res.*, **114**, D00A26, https://doi.org/10.1029/2007JD009755.

Maley, J., and E. Hilaire, 1993: The role of clouds in the evolution of tropical African palaeoenvironments. *Veille climatique satellitaire*, **46**, 51–63.

Mallet, M., P. Nabat, B. Johnson, M. Michou, J. M. Haywood, C. Chen, and O. Dubovik, 2021: Climate models generally underrepresent the warming by Central Africa biomass-burning aerosols over the Southeast Atlantic. *Sci. Adv.*, **7**, eabg9998, https://doi.org/10.1126/sciadv.abg9998.

Marchand, R., G. G. Mace, T. Ackerman, and G. Stephens, 2008: Hydrometeor detection using CloudSat—An Earth-orbiting 94-GHz cloud radar. *J. Atmos. Oceanic Technol.*, **25**, 519–533, https://doi.org/10.1175/2007JTECHA1006.1.

Met Office, 2012: Met Office Integrated Data Archive System (MIDAS) land and marine surface stations data (1853–current). NCAS British Atmospheric Data Centre, accessed 23 November 2021, https://catalogue.ceda.ac.uk/uuid/220a65615218d5c9cc9e4785a3234bd0.

Oliveira, R. S., C. B. Eller, P. R. L. Bittencourt, and M. Mulligan, 2014: The hydroclimatic and ecophysiological basis of cloud forest distributions under current and projected climates. *Ann. Bot.*, **113**, 909–920, https://doi.org/10.1093/aob/mcu060.

Painemal, D., K.-M. Xu, A. Cheng, P. Minnis, and R. Palikonda, 2015: Mean structure and diurnal cycle of southeast Atlantic boundary layer clouds: Insights from satellite observations and multiscale modeling framework simulations. *J. Climate*, **28**, 324–341, https://doi.org/10.1175/JCLI-D-14-00368.1.

Philippon, N., and Coauthors, 2019: The light-deficient climates of western Central African evergreen forests. *Environ. Res. Lett.*, **14**, 034007, https://doi.org/10.1088/1748-9326/aaf5d8.

——, A. Ouhechou, P. Camberlin, J. Trentmann, A. H. Fink, J. D. Maloba, B. Morel, and G. Samba, 2022: Characterization of sunshine duration in western equatorial Africa: In situ measurements versus SARAH-2 satellite estimates. *J. Appl. Meteor. Climatol.*, **61**, 185–201, https://doi.org/10.1175/JAMC-D-21-0072.1.

Räisänen, P., H. W. Barker, M. F. Khairoutdinov, J. Li, and D. A. Randall, 2004: Stochastic generation of subgrid-scale cloudy columns for large-scale models. *Quart. J. Roy. Meteor. Soc.*, **130**, 2047–2067, https://doi.org/10.1256/qj.03.99.

Schmetz, J., P. Pili, S. Tjemkes, D. Just, J. Kerkmann, S. Rota, and A. Ratier, 2002: An introduction to Meteosat Second Generation (MSG). *Bull. Amer. Meteor. Soc.*, **83**, 977–992, https://doi.org/10.1175/BAMS-83-7-Schmetz-2.

Schrage, J. M., and A. H. Fink, 2012: Nocturnal continental low-level stratus over tropical West Africa: Observations and possible mechanisms controlling its onset. *Mon. Wea. Rev.*, **140**, 1794–1809, https://doi.org/10.1175/MWR-D-11-00172.1.

Schuster, R., A. H. Fink, and P. Knippertz, 2013: Formation and maintenance of nocturnal low-level stratus over the southern West African monsoon region during AMMA 2006. *J. Atmos. Sci.*, **70**, 2337–2355, https://doi.org/10.1175/JAS-D-12-0241.1.

Smith, A., N. Lott, and R. Vose, 2011: The integrated surface database: Recent developments and partnerships. *Bull. Amer. Meteor. Soc.*, **92**, 704–708, https://doi.org/10.1175/2011BAMS3015.1.

Solmon, F., N. Elguindi, M. Mallet, C. Flamant, and P. Formenti, 2021: West African monsoon precipitation impacted by the south eastern Atlantic biomass burning aerosol outflow. *npj Climate Atmos. Sci.*, **4**, 54, https://doi.org/10.1038/s41612-021-00210-w.

Stephens, G. L., and Coauthors, 2002: The CloudSat mission and the A-Train: A new dimension of space-based observations of clouds and precipitation. *Bull. Amer. Meteor. Soc.*, **83**, 1771–1790, https://doi.org/10.1175/BAMS-83-12-1771.

van der Linden, R., A. H. Fink, and R. Redl, 2015: Satellite-based climatology of low-level continental clouds in southern West Africa during the summer monsoon season. *J. Geophys. Res. Atmos.*, **120**, 1186–1201, https://doi.org/10.1002/2014JD022614.

Wilson, A. M., and W. Jetz, 2016: Remotely sensed high-resolution global cloud dynamics for predicting ecosystem and biodiversity distributions. *PLOS Biol.*, **14**, e1002415, https://doi.org/10.1371/journal.pbio.1002415.

Winker, D. M., J. R. Pelon, and M. P. McCormick, 2003: The CALIPSO mission: Spaceborne lidar for observation of aerosols and clouds. *Third Int. Asia-Pacific Environmental Remote Sensing Remote Sensing of the Atmosphere, Ocean, Environment, and Space*, U. N. Singh, T. Itabe, and Z. Liu, Eds., International Society for Optical Engineering, 1–11, https://doi.org/10.1117/12.466539.

WMO, 2019: Identifying the genus. International Cloud Atlas, accessed 21 October 2021, https://cloudatlas.wmo.int/en/identifying-the-genus.html.

Wood, R., 2012: Stratocumulus clouds. *Mon. Wea. Rev.*, **140**, 2373–2423, https://doi.org/10.1175/MWR-D-11-00121.1.

Wood, T. E., M. A. Cavaleri, and S. C. Reed, 2012: Tropical forest carbon balance in a warmer world: A critical review spanning microbial-to ecosystem-scale processes. *Biol. Rev.*, **87**, 912–927, https://doi.org/10.1111/j.1469-185X.2012.00232.x.